J. Fluid Mech. (1990), *vol.* 220, *pp.* 569–594
Printed in Great Britain

The evolution of a localized disturbance in a laminar boundary layer. Part 1. Weak disturbances

By KENNETH S. BREUER† AND JOSEPH H. HARITONIDIS
Department of Aeronautics and Astronautics, Massachusetts Institute of Technology, Cambridge, MA 02139, USA

(Received 31 August 1989 and in revised form 5 April 1990)

The evolution of a low-amplitude localized disturbance in a laminar boundary layer is considered. Linear inviscid theory illustrates that the disturbance may be divided into two parts: a dispersive wave part, represented by solutions to the Rayleigh equation which travel at their characteristic speeds, and a transient or advective part travelling at the local mean velocity. For a three-dimensional initial disturbance, calculations based on linear inviscid theory indicate that the transient portion of the disturbance does not decay and has the form of an inclined shear layer which elongates as the disturbance propagates downstream. The amplitude of the transient part exceeds by far that of the wave part of the disturbance. Experimental results are presented for a disturbance created by the impulsive motion of a small membrane flush-mounted at the wall. For small amplitudes, the initial evolution of the disturbance is found to be in good qualitative agreement with the inviscid calculations, showing the rapid formation of an inclined shear layer. Further downstream, the transient portion of the disturbance decays owing to viscous effects, leaving a linearly unstable dispersive wave packet. The evolutions of equal and opposite disturbances are compared and it is shown that, despite a weak nonlinearity that develops, the resultant wave packets are equal in structure but of opposite phase.

1. Introduction

The breakdown of a laminar boundary layer to a turbulent flow has been an intensely studied subject during the past century. Much of the research has concentrated on the evolution of two-dimensional Tollmien–Schlichting waves whose growth is initially governed by the Orr–Sommerfeld equation. Above a critical Reynolds number, these waves grow and after a short time they reach finite amplitudes and are subject to nonlinear effects and various types of three-dimensional secondary instabilities. This route to transition has been well documented both in experiment and in theory (see, for example, Klebanoff, Tidstrom & Sargent 1962; Kovasznay, Komoda & Vasudeva 1962; Craik 1971; Herbert 1984).

While it is a natural starting point for a stability analysis, this approach has some limitations since it is not a very accurate approximation of what one might expect in a variety of physical situations. A naturally occurring flow is unlikely to experience two-dimensional uniform disturbances, but might be subjected to isolated, impulsive three-dimensional disturbances. On an aircraft wing, for example, such disturbances might originate from an imperfection on the wing surface, or from

† Present address: Center for Fluid Mechanics, Turbulence and Computation, Box 1966, Brown University, Providence, RI 02912, USA.

localized upstream irregularities, acoustic sources, etc. For this reason, it would seem appropriate to extend the two-dimensional analysis to three-dimensional, impulsive disturbances. In addition to this, the growth rates predicted by two-dimensional linear theory are very small, and a linear wave must travel a considerable distance before it reaches sufficient amplitudes for nonlinear effects to become important. In contrast, we shall show that localized disturbances can exhibit very rapid growth rates, even by linear mechanisms, entirely due to their initial three-dimensional nature.

There are several features that become apparent when one considers a single disturbance localized in both space and time. Orr (1907) discussed the initial value problem in an inviscid flow and pointed out that in addition to the discrete spectrum whose modes are eigensolutions to the Rayleigh equation, a continuous spectrum of modes must also be considered in order to account for any general initial disturbance. The continuous spectrum is a result of the exclusion of viscosity in the critical layer where the wave speed matches the local mean velocity. In a viscous flow, however, this singularity is no longer present and for bounded flows, such as plane Poiseuille flow, the discrete modes form a complete system (cf. DiPrima & Habetler 1969). However, for unbounded domains such as the flat plate boundary layer, Gustavsson (1978) showed that a 'viscous' continuous spectrum exists and is associated with the infinite (or semi-infinite) domain. The viscous continuous spectrum was also derived and studied by Grosch & Salwen (1978) who calculated the continuum eigenfunctions for both the Blasius boundary layer and the plane jet. The relationship between the spectra of the inviscid and viscous problems for the boundary layer has not been rigorously established, although studies (Lin 1955; Mack 1976; Antar & Benek 1978; Gustavsson 1978) suggest that as the Reynolds number increases, one Orr–Sommerfeld mode approaches the inviscid Rayleigh mode while the higher modes tend towards a neutrally stable inviscid continuum. In the following discussion, care must be taken not to confuse the inviscid continuous spectrum with the viscous continuous spectrum.

Case (1960) outlined the solution for a general two-dimensional inviscid parallel flow, and he distinguished between the discrete modes derived from the conventional normal mode analysis and those modes associated with the inviscid continuous spectrum. His asymptotic analysis for the continuous modes at large times indicated that they decay as $1/t$. Gustavsson extended this work to three-dimensional disturbances in a piecewise linear boundary layer and found that the vertical velocity, v, could be represented by a dispersive part associated with the solution to the Rayleigh equation and also a part resulting from the inviscid continuous spectrum which he termed the convected part because it travels at the local mean velocity of the flow. For the vertical velocity component, Gustavsson found that, for two- and three-dimensional disturbances, both of these parts decayed as $1/t^2$ for fixed values of x and t, and as $1/t$ in a coordinate system moving with the disturbance.

For a two-dimensional flow, the streamwise velocity is directly related to the vertical velocity through continuity, and so the results for v also apply to the streamwise disturbance velocities. However, for an initial disturbance with a spanwise structure, Gustavsson confirmed Landahl's (1975) result that the streamwise component of velocity included a term which did not vanish at large times. This *permanent scar*, as Landahl has termed it, is an advective term (i.e. it travels at the local mean velocity) and is solely a result of the three-dimensional nature of the initial disturbance. Landahl (1984) further examined this effect in which the integrated effect of the vertical perturbation velocity displaces fluid

particles in the vertical direction. If there is a mean shear, this 'liftup' creates a horizontal disturbance velocity which will not, in general, disappear for long times. Landahl (1980) also showed that any general three-dimensional disturbance, subject to some constraints, gives rise to an algebraic instability in which the energy of the disturbance will grow at least as fast as linearly in time. This behaviour is in strict contrast to the two-dimensional theory which predicts that the transient modes decay.

Gustavsson's (1978) approach was followed by Henningson (1988) who examined the initial-value problem for a piecewise linear plane Poiseuille flow. Henningson solved the initial-value problem numerically and computed the flow field for a specific initial disturbance. His results also showed that the transient modes dominate over the dispersive modes after a short time, forming an internal shear layer which intensifies as the disturbance evolves.

By examining the evolution of such localized disturbances in a laminar boundary layer, we are extending the analysis of Henningson (1988) to the flat-plate geometry. We first consider the numerical solution of the linear inviscid initial-value problem for the flat-plate boundary layer. Although this approximation is an extreme simplification, it is useful since it clearly shows the distinction between the wave and transient parts of the localized disturbance. The approximation is valid for moderate times since the mechanisms that we are interested in, namely the liftup effect and the role of the transient part of the disturbance, are governed by linear inviscid mechanisms which act over short times. As the results of §2 show, the three-dimensional transient effects dominate the evolution of the initial disturbance while the wave portion of the disturbance, although present, does not significantly contribute to the structure of the disturbance.

In §3, we present some results from experimental measurements of the evolution of an artificially triggered localized disturbance in a laminar boundary layer at $Re_{\delta^*} = 950$. The experimental conditions are such that the measurements and the linear theory may be compared, and considerable care was taken so that the initial disturbance produced in the experiments and the initial conditions used in the linear calculations were of similar structure and scale, and that the amplitude of the initial disturbance generated in the wind tunnel was small enough that linear mechanisms dominated the disturbance's evolution. Although the results of the theory do compare well in many respects with those of the experiment, there are important differences between the two, especially in the long-time behaviour of the disturbance. These issues will be addressed more fully in §3 in which we show that the effect of viscosity on a 'weak' initial perturbation is to cause the eventual decay of the transient part of the disturbance (the inclined shear layer), leaving only a dispersive wave packet which grows slowly as it travels downstream. For higher-amplitude initial disturbances, the transient does not decay and nonlinear effects lead to the direct breakdown of the disturbance to a turbulent spot, bypassing the wave packet stage. These 'strong' disturbances are considered in an accompanying paper (Breuer & Landahl 1990).

2. Linear theory

2.1. *Derivation of equations*

The derivation of the equations for the linear, inviscid initial-value problem is straightforward and our approach follows previous discussions of the problem (e.g. Case 1960; Drazin & Reid 1981; Gustavsson 1978; Henningson 1988). Although the

analysis is not new and closely follows that due to Henningson, we present it here for completeness and convenience. In this analysis, the flow is assumed to be inviscid and the mean flow is taken to be two-dimensional and parallel, ignoring the effects of the downstream growth of the boundary layer. This assumption is valid for moderate times of evolution since the boundary-layer thickness increases with the square root of downstream distance and for the cases investigated here ($x_0 = 0.76$ m, $R_{\delta^*} = 1000$ in the experimental results reported in §3) the boundary-layer thickens only 8% over a distance of $50\delta^*$.

The linearized, inviscid, three-dimensional equations of motion are:

$$u_t + Uu_x + U'v = -p_x, \tag{1}$$

$$v_t + Uv_x = -p_y, \tag{2}$$

$$w_t + Uw_x = -p_z, \tag{3}$$

$$u_x + v_y + w_z = 0. \tag{4}$$

Here, x represents the streamwise direction, y the direction normal to the wall and z the spanwise direction. u, v, w and p represent the three perturbation velocities (in the streamwise, vertical and spanwise directions respectively) and the perturbation pressure. $U(y)$ is the mean flow and a prime denotes a derivative with respect to the vertical direction y. After taking the Fourier transform in the x- and z-directions, we can derive an equation for the transformed pressure,

$$\tilde{p} = \frac{1}{k^2}\left[\mathrm{i}\alpha U'\tilde{v} - \left(\frac{\partial}{\partial t} + \mathrm{i}\alpha U\right)\tilde{v}_y\right], \tag{5}$$

where a tilde represents a transformed quantity. α is the streamwise wavenumber, β is the spanwise wavenumber and $k^2 = \alpha^2 + \beta^2$. After taking the y-derivative of this and substituting into the vertical momentum equation, we get the familiar Rayleigh equation for the vertical velocity $\tilde{v}$,

$$\left(\frac{\partial}{\partial t} + \mathrm{i}\alpha U\right)\left(\frac{\partial^2}{\partial y^2} - k^2\right)\tilde{v} - \mathrm{i}\alpha U''\tilde{v} = 0. \tag{6}$$

The equation may be solved, subject to the usual boundary conditions, namely that v vanish at the wall and decay exponentially in the free stream, $v \propto \mathrm{e}^{-ky}$. As was previously mentioned, the general solution to the Rayleigh equation includes both a dispersive term, deriving from the eigenmodes of the equation, and an advective or 'transient' term resulting from the inviscid continuous spectrum of the Rayleigh equation. Unlike the inviscid eigenmodes for the Blasius profile which are damped, the transient portion of the disturbance is neutrally stable (c must be real for $U(y) - c = 0$). Gustavsson (1978) has also shown that the transient portion of v travels at the local mean velocity (rather than at the dispersive wave speeds associated with the normal modes) and decays as $1/t^2$, both for two- and three-dimensional disturbances.

One can also obtain equations for the horizontal velocity components:

$$\left(\frac{\partial}{\partial t} + \mathrm{i}\alpha U\right)\tilde{u} = -\frac{\beta^2}{k^2}U'\tilde{v} + \frac{\mathrm{i}\alpha}{k^2}\left(\frac{\partial}{\partial t} + \mathrm{i}\alpha U\right)\tilde{v}_y, \tag{7}$$

$$\left(\frac{\partial}{\partial t} + \mathrm{i}\alpha U\right)\tilde{w} = \frac{\alpha\beta}{k^2}U'\tilde{v} + \frac{\mathrm{i}\beta}{k^2}\left(\frac{\partial}{\partial t} + \mathrm{i}\alpha U\right)\tilde{v}_y. \tag{8}$$

Following Henningson (1988), we can simplify these equations by rotating the horizontal axes so that they are aligned with the wave vector defined by α and β. The transformation is defined as

$$\tilde{u}_1 = \frac{1}{k}(\alpha\tilde{u} + \beta\tilde{w}), \tag{9}$$

$$\tilde{w}_1 = \frac{1}{k}(\beta\tilde{u} - \alpha\tilde{w}), \tag{10}$$

in which $\tilde{u}_1$ is the velocity component perpendicular to the wave front and $\tilde{w}_1$ is the component parallel to the wave front. This transformation also serves to separate the two- and three-dimensional effects since $\tilde{u}_1$ is the component of velocity driven via continuity, while $ik\tilde{w}_1$ is the vertical vorticity. Applying this transformation to (7) and (8), we obtain

$$\left(\frac{\partial}{\partial t} + i\alpha U\right)\tilde{u}_1 = \frac{i}{k}\left(\frac{\partial}{\partial t} + i\alpha U\right)\tilde{v}_y, \tag{11}$$

$$\left(\frac{\partial}{\partial t} + i\alpha U\right)\tilde{w}_1 = -\frac{\beta}{k}U'\tilde{v}. \tag{12}$$

These equations can be integrated directly using appropriate initial conditions (denoted by a zero subscript) yielding:

$$\tilde{u}_1 = \frac{i}{k}\tilde{v}_y, \tag{13}$$

$$\tilde{w}_1 = \tilde{w}_{1_0} e^{-i\alpha U(y)t} - \frac{\beta}{k}U' e^{-i\alpha U(y)t}\int_0^t \tilde{v}(y,t') e^{i\alpha U(y)t'}\,dt'. \tag{14}$$

The original velocity components can be retrieved by solving (9) and (10):

$$\tilde{u} = \frac{1}{k}(\alpha\tilde{u}_1 + \beta\tilde{w}_1), \tag{15}$$

$$\tilde{w} = \frac{1}{k}(\beta\tilde{u}_1 - \alpha\tilde{w}_1). \tag{16}$$

The equations for $\tilde{u}_1$ and $\tilde{w}_1$, (13) and (14), clearly illustrate the additional term that the three-dimensionality introduces in the evolution of a disturbance. The expression for $\tilde{u}_1$ is simply a statement of continuity in the plane of the wavefront and this component of velocity is determined directly from the solution to the Rayleigh equation. Since the vertical velocity decays, so must this portion of the disturbance. The vertical vorticity, proportional to $\tilde{w}_1$, has a markedly different character. The first term represents the advection of the initial vertical vorticity field at the local mean velocity. The second term in the expression for $\tilde{w}_1$, which depends on β, the mean shear and the integrated effect of the vertical velocity, is the so-called 'liftup' term since it represents the *generation* of horizontal velocity perturbations by the lifting-up of fluid elements in the presence of the mean shear. In contrast to the behaviour of $\tilde{u}_1$, one can show that this term does not decay (Landahl 1975; Gustavsson 1978) and gives rise to large-amplitude, growing, perturbations in the horizontal velocity components despite the fact that v decays and that the Rayleigh equation only admits solutions which are, at best, neutrally stable. Landahl (1980) has also shown that if

$$\int_{-\infty}^{\infty} v_0\,dx \neq 0 \tag{17}$$

(that is, if the initial disturbance contains energy at $\alpha = 0$) then the disturbance energy grows at least as fast as linearly in time owing to the elongation of the disturbance as it travels downstream. The liftup concept is somewhat analogous to Prandtl's mixing-length hypothesis for the generation of Reynolds stresses in a turbulent shear flow. However, that idea does not derive from any three-dimensional arguments, whereas the liftup term described here is solely due to three-dimensional effects. One should note that for a more compact spanwise structure (i.e. for larger values of β) and for a stronger mean shear this effect will become more pronounced.

In order to fully solve (6), (11) and (12) either some simplifying assumptions must be made about the mean profile or the initial conditions, or one must resort to numerical methods of solution. Both Gustavsson (1978) and Henningson (1988) assumed piecewise linear profiles for the mean velocity profiles in a boundary layer and a plane Poiseuille flow respectively, and with that simplification they were able to integrate the equations in closed form. The strength of this approach is that the different effects present in the solution are readily seen in the analytical solution, but the treatment of the mean profile by a series of linear segments does introduce some spurious behaviour in the solution, especially in the dispersive part, which is quite sensitive to the mean profile curvature, which has now been concentrated into a series of delta functions located at the profile's break points. Henningson's results indicate that while the wave speed for the symmetric mode was quite well represented by a piecewise approximation of the plane Poiseuille profile, the antisymmetric mode was in considerable error. Only by considering the complete profile can the dispersive behaviour be accurately treated and so for the present work the complete Blasius profile was used, and the equations were integrated directly using a finite-difference technique described in the following subsection.

2.2. *Numerical method*

The Rayleigh equation (6) was solved by dividing it into two equations:

$$\frac{\partial \nabla^2 \tilde{v}}{\partial t} = \mathrm{i}\alpha(U''\tilde{v} - U\nabla^2\tilde{v}), \tag{18}$$

$$\nabla^2\tilde{v} = \left(\frac{\partial^2}{\partial y^2} - k^2\right)\tilde{v}. \tag{19}$$

This equation was discretized into J points in the normal direction, and second-order finite differences were used to evaluate the vertical derivatives. A Crank–Nicolson scheme was used to march forward in time, ensuring stability. The resulting finite-difference equations obtained are

$$\nabla^2\tilde{v}_j^{n+1} - \nabla^2\tilde{v}_j^n = \tfrac{1}{2}\mathrm{i}\alpha\Delta t[U_j''(\tilde{v}_j^{n+1} + \tilde{v}_j^n) - U_j(\nabla^2\tilde{v}_j^{n+1} + \nabla^2\tilde{v}_j^n)], \tag{20}$$

$$\nabla^2\tilde{v}^n = \frac{\tilde{v}_{j+1}^n - 2\tilde{v}_j^n + \tilde{v}_{j-1}^n}{\Delta y^2} - k^2\tilde{v}_j^n, \tag{21}$$

where the superscript refers to the current time step and the subscript refers to the vertical level. This system of equations may be written in matrix form for the vector $\tilde{\boldsymbol{v}}^n$ which represents the complete vertical disturbance velocity at time step n: $\tilde{v}_j^n, j = 1 \ldots J$. Writing the equations in this form and after some simple matrix operations we obtain:

$$(\boldsymbol{I} + \mathrm{i}\boldsymbol{R})\boldsymbol{D}\tilde{\boldsymbol{v}}^{n+1} = (\boldsymbol{I} - \mathrm{i}\boldsymbol{R})\boldsymbol{D}\tilde{\boldsymbol{v}}^n + \mathrm{i}\boldsymbol{S}(\tilde{\boldsymbol{v}}^{n+1} + \tilde{\boldsymbol{v}}^n) \tag{22}$$

where $\boldsymbol{R}$ and $\boldsymbol{S}$ are diagonal matrices associated with the mean profile:

$$\boldsymbol{R} = \tfrac{1}{2}\mathrm{i}\alpha\Delta t U_j \boldsymbol{I} \tag{23}$$

$$\boldsymbol{S} = \tfrac{1}{2}\mathrm{i}\alpha\Delta t U_j'' \boldsymbol{I}. \tag{24}$$

$\boldsymbol{D}$ is the (tri-diagonal) matrix associated with the Laplacian derivative in the normal direction (21) and $\boldsymbol{I}$ is the identity matrix. After some further simple manipulations, we arrive at an equation for advancing the vertical disturbance velocity in time:

$$\tilde{\boldsymbol{v}}^{n+1} = (\boldsymbol{D}+\mathrm{i}(\boldsymbol{RD}-\boldsymbol{S}))^{-1}(\boldsymbol{D}-\mathrm{i}(\boldsymbol{RD}-\boldsymbol{S}))\,\tilde{\boldsymbol{v}}^{n}. \tag{25}$$

It should be noted that for fixed α, β and Δt, all of these matrices are constant and need to be evaluated and combined only once, at $t = 0$. In order to calculate the disturbance velocity at any subsequent time we need only apply the resultant matrix iteratively to the $\tilde{\boldsymbol{v}}^n$ array. A variable spacing in the y-direction may be incorporated in the $\boldsymbol{D}$-matrix, allowing for additional resolution near the wall. Since the matrices are all tri-diagonal, this allows for very fast manipulation and inversion during the computational cycle.

The equation for the array $\tilde{\boldsymbol{w}}_1$, proportional to the vertical vorticity $\tilde{w}_1$, (12), can also be written in matrix form:

$$(\boldsymbol{I}+\mathrm{i}\boldsymbol{R})\,\tilde{\boldsymbol{w}}_1^{n+1} = (\boldsymbol{I}-\mathrm{i}\boldsymbol{R})\,\tilde{\boldsymbol{w}}_1^{n} - \boldsymbol{T}(\tilde{\boldsymbol{v}}^{n+1}+\tilde{\boldsymbol{v}}^{n}) \tag{26}$$

where the matrix $\boldsymbol{R}$ is as defined in (23) and $\boldsymbol{T}$ is another constant diagonal matrix:

$$\boldsymbol{T} = \frac{\Delta t\beta U'}{2k}\boldsymbol{I}. \tag{27}$$

This equation may be integrated at the same time as the Rayleigh equation (25) utilizing the current values for $\tilde{\boldsymbol{v}}^n$ and $\tilde{\boldsymbol{v}}^{n+1}$.

Since the resultant velocity field must be a real quantity, each velocity component must have symmetry across the complex plane: $\tilde{u}(\alpha,\beta) = \tilde{u}^*(-\alpha,-\beta)$, where a star denotes the complex conjugate (similarly for $\tilde{v}$ and $\tilde{w}$). Thus, only positive values of α need to be considered. For the results presented here, the disturbance was assumed to be symmetric about $z = 0$, and therefore the equations were solved using only positive values of β.

2.3. *Initial conditions*

The initial disturbance was chosen so as to be localized, to satisfy continuity, and to be a good approximation to the initial disturbance produced in the experiments described in §3 in which a flush-mounted membrane was impulsively moved up and then down, generating a localized vertical motion. In order to simulate this motion, the initial conditions used (shown in figure 1) had the form of a pair of counter-rotating streamwise vortices. This disturbance, identical to the one used by Russell & Landahl (1984) and similar to that used by Henningson (1988), is derived from a two-dimensional stream function:

$$u = 0; \quad v = -\frac{\partial \Psi}{\partial z}; \quad w = \frac{\partial \Psi}{\partial y}, \tag{28}$$

where

$$\Psi = \bar{x}\bar{z}\bar{y}^3\,\mathrm{e}^{-\bar{x}^2-\bar{y}^2-\bar{z}^2} \tag{29}$$

and $\bar{x}, \bar{y}, \bar{z}$ are the normal Cartesian coordinates scaled by some characteristic lengths l_x, l_y and l_z:

$$\bar{x} = x/l_x; \quad \bar{y} = y/l_y; \quad \bar{z} = z/l_z. \tag{30}$$

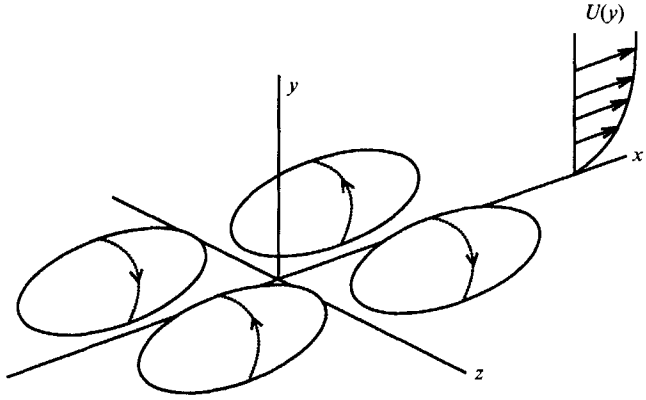

FIGURE 1. Schematic of the initial perturbation used in the numerical studies to simulate the membrane motion used in the experiment. The perturbation represents two pairs of counter-rotating streamwise vortices.

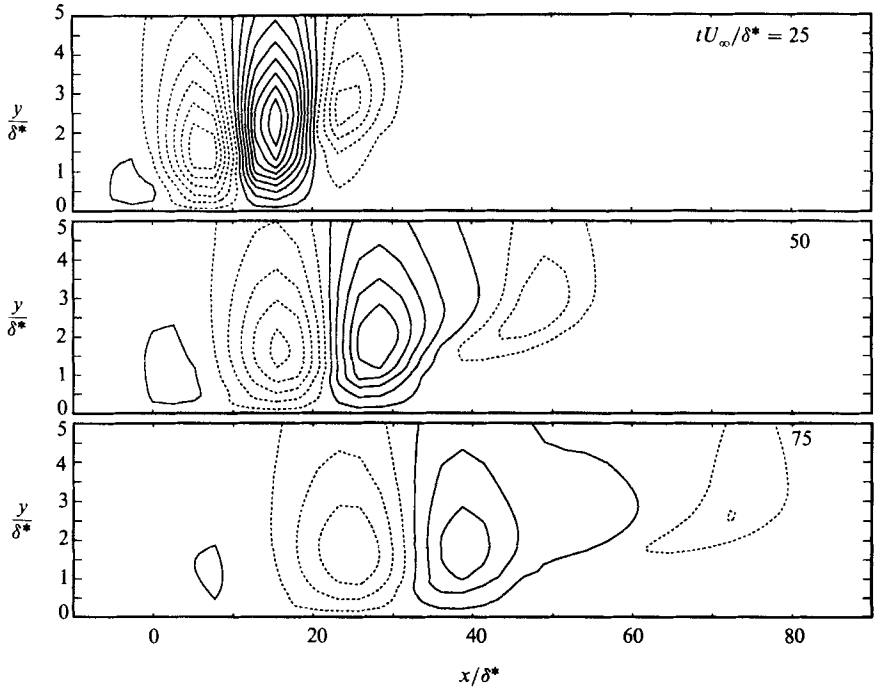

FIGURE 2. Linear initial-value problem. Contours of vertical velocity in the (x, y)-plane at $z = 0$. Contour spacing: 0.2 of the maximum initial v-perturbation. In this and subsequent similar figures, solid lines represent positive contours, dotted lines represent negative contours.

For the present results, the scaling lengths used were: $l_x = 5\delta^*$, $l_y = 1.2\delta^*$, and $l_z = 6\delta^*$. These were chosen so as to best approximate the scale of the disturbance produced in the experiments described in §3. At $t = 0$ the centre of the disturbance is located at $x = 0, z = 0$.

2.4. *Results and discussion*

The system described by (25) and (26) was solved numerically using standard routines for tri-diagonal matrices. The calculation used 64 modes in α and 32 modes in β. The computational domain was a box, $200\delta^*$ in the streamwise direction and $50\delta^*$ in the spanwise direction. The vertical direction was discretized into 41 equally

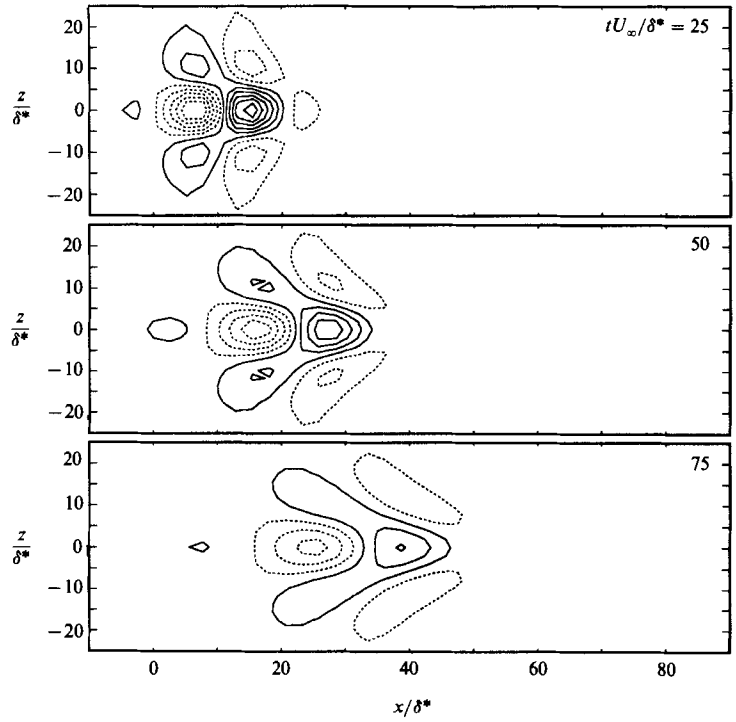

FIGURE 3. Linear initial-value problem. Contours of vertical velocity in the (x,z)-plane at $y/\delta^* = 1$. Contour spacing: 0.2 of the maximum initial v-perturbation.

spaced points from $y/\delta^* = 0$ to 6. For each combination of α and β, the equations were integrated from $t = 0$ to the desired time, using the analytic Fourier transform of the above-described initial perturbation as the initial condition. Fast Fourier transforms were used to convert the final results back to physical space.

The vertical component of velocity is shown in figures 2 and 3, which show the evolution of v in the (x,y)-plane at $z = 0$ and in the (x,z)-plane at $y/\delta^* = 1$ respectively. In these figures, and for all subsequent results, the axes are scaled by the displacement thickness, δ^*, and the flow is from left to right. The edge of the boundary layer is located at approximately $3\delta^*$. The v-component is only dependent on the solution to the Rayleigh equation (6) and it illustrates both the transient and the dispersive characters of the solution. In figure 2, the overall coherence of the v-component through the boundary layer, and the apparent exponential decay of the perturbations outside the boundary layer, reflect the familiar behaviour of the wave modes that are usually considered in stability calculations. The only visible sign of the transient modes is the patch of low-speed fluid that pulls ahead of the disturbance, travelling high in the boundary layer and at speeds comparable with the free-stream velocity. With the exception of the exponential decay in the free stream, the structure of v at $t = 25$ strongly resembles that of the initial conditions at $t = 0$. This is also indicated in figure 3, although at later times the decay of the disturbance and its increasing wave-packet-like character become evident as it travels downstream.

Figure 4 shows the streamwise perturbation velocity, plotted on the centreline in the (x,y)-plane, and we immediately see the difference between the u- and the v-components due to the vertical vorticity term. Although there is no u-perturbation

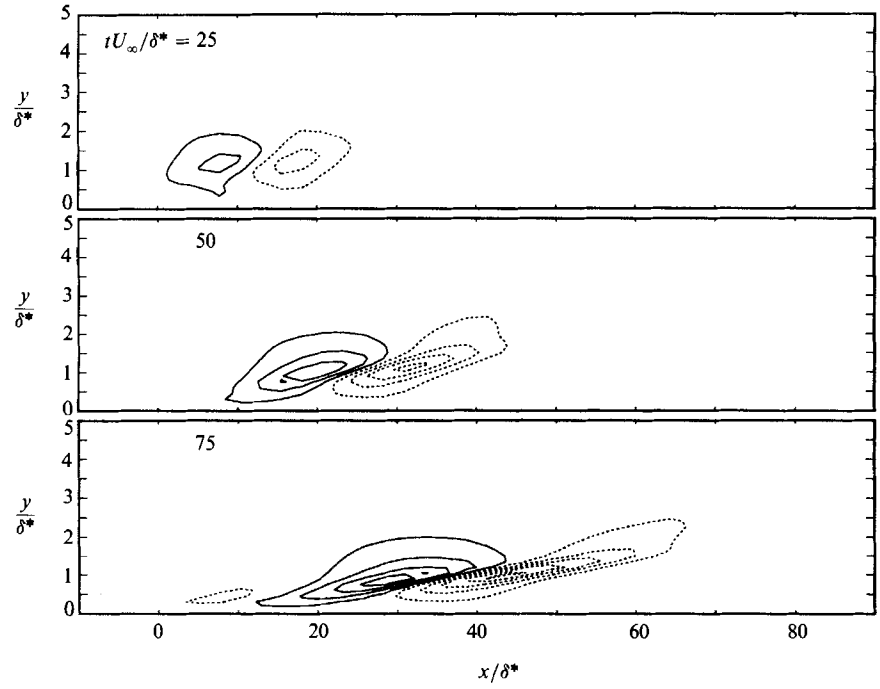

FIGURE 4. Linear initial-value problem. Contours of streamwise perturbation velocity in the (x, y)-plane at $z = 0$. Contour spacing: twice the maximum initial v-perturbation.

initially, a strong streamwise perturbation velocity quickly develops, forming a low-speed region immediately followed by a high-speed region of fluid. As the disturbance travels downstream, the whole structure is tilted over and stretched so that an internal shear layer forms which intensifies as the disturbance evolves. The structure of the disturbance illustrates the dominant nature of the liftup effect that is unique to three-dimensional disturbances. The form of the initial vertical velocity pushes up low-speed fluid at the front of the disturbance and pulls down high-speed fluid in the rear through the mechanism for generation of vertical vorticity via the liftup term. This initial vertical motion creates the observed streamwise perturbations. Because the transient part of the disturbance travels at the local mean velocity, the upper part of the disturbance advects faster than the part closer to the wall, resulting in the tilting of the shear layer, the stretching of the structure in the streamwise direction and, consequently, the intensification of the shear layer as time advances. In contrast to the character of v, the u-perturbations are confined to the boundary-layer region and do not extend beyond the region of mean shear. This is understandable, knowing that the liftup term (14) is only non-zero when there is a mean shear. Since there is no viscosity to limit the shear-layer thickness by diffusion of the local vorticity, the shear layer continues to intensify with increasing time.

Although this is an inviscid calculation in which free modes are damped and the continuum modes are neutrally stable, the rapid growth of the disturbance emphasizes that this mechanism is not due to a conventional instability, but rather to the continued liftup of fluid elements by the v-component of the initial disturbance and the subsequent generation of vertical vorticity. As the amplitude of v decays owing to dispersion (see figure 6), this liftup will decrease, and at that point the disturbance amplitude will not increase any further.

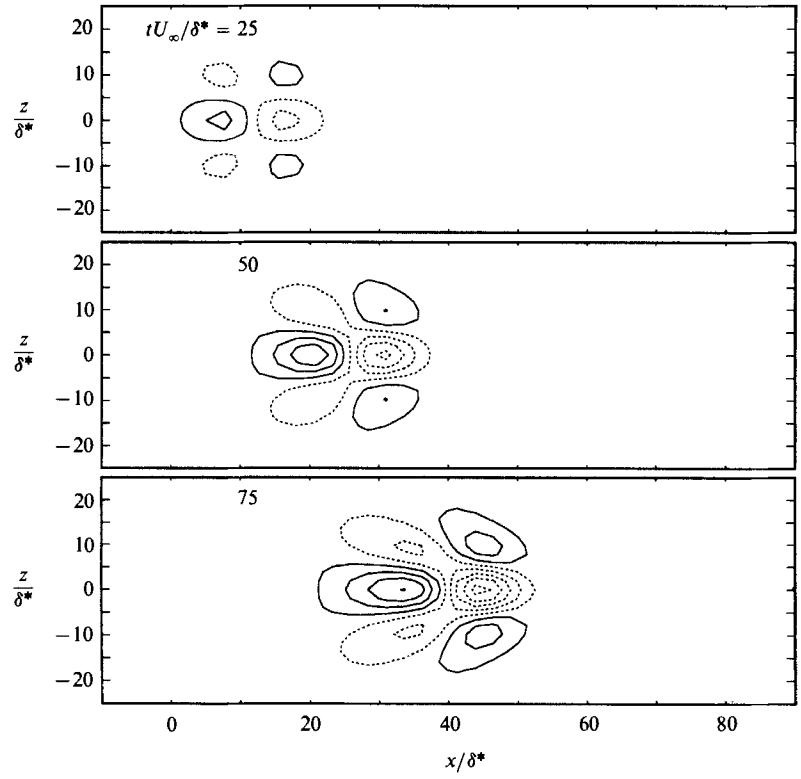

FIGURE 5. Linear initial-value problem. Contours of streamwise perturbation velocity in the (x, z)-plane at $y/\delta^* = 1$. Contour spacing: twice the maximum initial v-perturbation.

The spanwise structure calculated by the linear theory is shown in figure 5, which depicts a horizontal cut through the boundary layer at $y/\delta^* = 1$. The initial perturbation field also confirms the primary effect of the liftup of fluid elements by the initial velocity field. The low-speed–high-speed pattern in u exactly matches the areas where the initial v-field was positive and negative respectively. As the disturbance evolves, the central core of the disturbance intensifies as indicated in figure 4, but a new feature observed is the developing wave field seen at the edges of the disturbance. This is the dispersive part of the disturbance emerging, driven by the wave portion of the v-component. Since the transient portion of the disturbance is advected by the mean field, it cannot spread laterally. The wave part, however, does disperse in the spanwise direction, and thus, at the later times, it becomes visible at the edges of the disturbance field where the transient modes are not so dominant.

The amplitude evolution of the disturbance is summarized in figure 6, which shows the maximum disturbance amplitude in the entire field as a function of time. From $tU/\delta^* = 0$ to about 40, the growth is linear and this growth is due to the initial liftup of fluid elements by the vertical velocity. For larger times, v decays as we would expect and, consequently, the growth in the horizontal velocities slows. The u-component growth never completely levels off since the v-component does not decay very fast and so a relatively long time is required for the liftup process to finish. As discussed earlier, the v-component should decay as $1/t$ in a frame of reference moving with the disturbance. Examination of the amplitude of v indicates that this decay

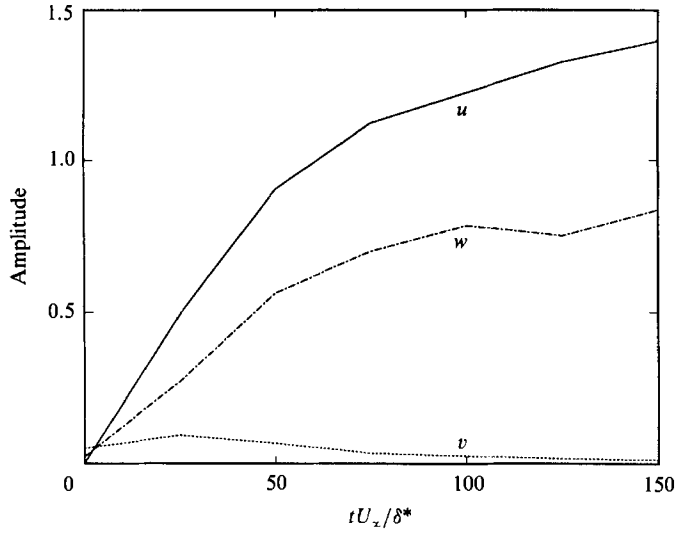

FIGURE 6. Linear initial-value problem. Maximum peak-to-peak amplitude of the perturbation velocities u, v and w as a function of time.

rate is well reproduced by the present results. The reason for the uneven behaviour of the w-component at large times is unclear, although the spreading of the disturbance might affect the solution at the later times through the contamination of adjacent disturbances via the periodic boundary conditions.

The dominant effect of the three-dimensional terms on the disturbance is confirmed by considering solely the contribution to the streamwise perturbation velocity by the vertical vorticity. Equation (13) indicates that the $\tilde{u}_1$ component is directly coupled to the vertical velocity through continuity, and so we would expect that its contribution would quickly become negligible, since figure 6 indicates that the amplitude of v decays quite quickly. Indeed, if one sets $u_1 = 0$ and performs the inverse Fourier transform to see the velocity field due to the vertical vorticity at $tU/\delta^* = 75$, one finds that it is almost indistinguishable from the full velocity field shown in figure 5. This agrees very well with a similar result by Henningson (1988) for piecewise linear plane Poiseuille flow.

3. Experimental results

3.1. *Experimental set-up*

The experiments described were conducted in the Turbulence Research Laboratory in the department of Aeronautics and Astronautics at MIT. The details of the wind tunnel and the flat plate may be found in Mangus (1984), but we shall outline the pertinent features here. The wind tunnel is a closed-loop type with a test section 6.1 m long, 1.22 m high and 0.6 m wide. The flate plate, made from aluminium, is 12.7 mm thick and is mounted vertically, 10 cm from one of the tunnel sidewalls. The plate extends the entire length of the test section and to within 10 cm of both the tunnel floor and ceiling. The 10 cm gaps are covered by perforated metal sheets behind which are ducts for suction to control the growth of the boundary layers that grow in the corners of the test section. The corner flows grow substantially further downstream, and contaminate the boundary layer on the flat plate at large downstream distances. For the present experiments the corner contamination was

not a problem and the suction control was not used. A tapered leading edge with a rounded tip is attached to the front of the plate. The coordinate system and velocity notation is the same as that used in the numerical work discussed earlier.

The flow measurements were made using constant-temperature hot-wire anemometry. The hot-wire probes used, both for single-wire and two-wire measurements, were constructed in-house and typically had dimensions of less than 0.5 mm in length. 10% Pt–Rh wire, 1.27 μm in diameter, was used for the sensing wire, giving a typical length-to-diameter ratio greater than 300. The probes were operated at a resistive overheat of 30%. The anemometer circuits used were also built in-house. For measuring the u- and v-components of velocity, a standard $\times$-probe was built, having a box size of 0.4 mm while u and w were measured using a V-probe (a dual-wire probe in which the hot wires are arranged in the horizontal plane in a swept-back manner, approximately 45° to the oncoming flow).

The data was acquired using a Phoenix Data A/D system connected to a PDP-11/55 computer, which also controlled the probe positioning, timing, and all other aspects of the experiment. Subsequent data processing and graphics were performed on a MicroVax II. The hot-wire probe was mounted on a traversing mechanism with four degrees of freedom: x, y, z and one rotational axis for dual-wire calibration.

All hot-wire calibration was performed directly by the computer. No linearizers or signal conditioners were used. For single-probe measurements, the wire was calibrated by fitting seven calibration points to a cubic polynomial. For dual-wire measurements (both $\times$-wires for measuring u and v, and V-wires for measuring u and w) a look-up-table procedure was used. This method, based on one described in Lueptow, Breuer & Haritonidis (1988), generates a look-up table from the calibration data (taken at seven velocities and nine angles) and uses bi-linear interpolation to calculate the two components of velocity from a pair of raw hot-wire voltages E_1, E_2. Initial versions of the calibration procedure used the hot-wire voltages directly as the variables for a Cartesian look-up table, but for these results an improved procedure (Gresko 1988) was used. This method converts E_1 and E_2 into polar coordinates r, θ and thus takes advantage of the fan-like shape of the raw calibration data and allows for a more efficient use of the table and a more accurate calibration. In all cases, the error in the probe calibration $(u_{\text{meas}} - u_{\text{actual}})/u_{\text{actual}}$ was less than 0.5% in both u and v (or w). During the actual data acquisition, the hot-wire linearization was carried out by an assembly language routine on the PDP-11/55. This allowed for very fast conversion of the raw voltages to velocities, speeding up the data collection considerably. The calibration was checked frequently for drift to ensure that it was still valid, and provided that the tunnel and electronic equipment had been operating for some time and had achieved thermal equilibrium, the calibration typically remained accurate for several hours.

The form of the initial disturbance was of considerable importance. It was desirable to generate a simple, repeatable perturbation that contained the vital ingredient for the transient growth to be observed (localized initial vertical velocity). Simplicity was desired, both to allow a simple analytical representation of the disturbance in the calculations, and to enable the study of the three-dimensional effects with a minimum of other distracting phenomena. In their study of 'incipient spots', Amini & Lespinard (1982) used an air jet introduced through a 1 mm hole in the wall and driven by the action of an audio speaker. The disadvantage of this type of disturbances is that it is very small and concentrated. The small spanwise dimension of the disturbance makes the detailed measurement of its structure somewhat difficult, and it is desirable to generate a disturbance with a larger

spanwise dimension. Another problem is that the positive disturbance – generated by an upward motion of the speaker diaphragm which pushes air up through the hole – is completely different from the negative disturbance – generated by downward motion of the diaphragm which sucks air down through the hole. This difference between the two exists because the upward motion of the speaker results in a jet of air injected into the boundary layer, while the downward motion of the speaker creates a near-uniform sink flow from the boundary layer and down through the hole. For the experiments presented here, it was desirable to be able to produce a repeatable disturbance with a high degree of control over the amplitude and also to be able to produce disturbances identical in amplitude and structure, but with opposite sign. This latter requirement enables us to examine the effects of nonlinearity by comparing equal and opposite disturbances.

The disturbance generator used was a rectangular membrane with rounded edges, 9 mm by 17 mm, mounted flush with the wall at a distance of 0.76 m from the leading edge of the plate. The membrane was embedded into a circular plug and positioned so that the long dimension of the membrane was perpendicular to the direction of flow. A cavity below the membrane, approximately 3 mm deep, was connected through a three-port, solenoid-controlled valve to either a high- or a low-pressure source. When idle, the valve connected the cavity to the ambient pressure and the membrane lay flush with the wall. By activating the valve and exposing the membrane to the high-pressure source, the membrane deformed upwards, forming a small bump on the surface of the plate. Releasing the valve connected the cavity to the ambient pressure and allowed the membrane to return to its equilibrium position. The net effect was to produce a short, localized up–down motion at the wall. Similarly, by connecting the membrane to a low-pressure source, the membrane moved down when the valve was activated and a down–up wall motion could be achieved, producing the same disturbance but with opposite sign (this will be demonstrated in §3.5.3). The electric pulse to the solenoid-controlled valve could be varied so as to alter the duration of the wall motion. The shortest cycle time (governed by the physical response time of the valve) was found to be 4 ms, and this was achieved by operating the valve at 40 V (instead of the rated 12 V) in conjunction with a 200 Ω dropping resistor.

3.2. *Mean flow characteristics*

Extensive measurements were made to determine the quality of the mean flow in the test section. Two quantities were of special interest: the uniformity of the boundary layer across the span of the flat plate, and the extent to which the flow conformed to a Blasius boundary layer. The spanwise uniformity of the flow was characterized by measuring the displacement thickness (δ^*) at 1 cm intervals, from +40 to −40 cm, and at different x-locations. Initially, large and concentrated peaks in δ^* were discovered and it was found that the location of these peaks corresponded to the location of seams in the screens in the settling chamber of the wind tunnel. The peaks in δ^* remained confined to a very small spanwise extent (<1 cm) as far as 3 m downstream from the leading edge, and were accompanied by increased streamwise velocity fluctuation levels within the boundary layer. The last of four settling chamber screens was replaced, which removed the largest peaks, but some localized variations still persisted and despite extensive efforts, the cause of these peaks has yet to be determined. At $x = 1$ m, the variation of δ^* is typically confined to within 5% of its mean value, although at its worst point ($z = -12$ cm), δ^* rises 10% above the average value. One possible cause of these non-uniformities is that the seams of

x_0	0.76 mm
U_∞	6.0 m/s
δ^*	2.4 mm
δ_θ	0.9 mm
$\delta_{0.99}$	6.9 mm
Re_x	300000
Re_{δ^*}	950

TABLE 1. Flow parameters at the location of the disturbance generator for the experimental results (based on the Blasius solution for the boundary layer)

the screen created a wake with localized vorticity which then impinged on the plate at the leading edge and was stretched out in the streamwise direction. However, this does not explain the peaks present after the new screen was in place. An alternative explanation is that potential fluctuations from the boundary layer on the contraction wall (which was measured to be turbulent and of varying thickness across the span), were causing localized disturbances on the flat plate.

Despite these mean flow aberrations, the effect of the spanwise variations was not found to be serious. The variations in the base flow are not symmetrical about the centreline, and thus any effect they may have had on the measurements should have been detectable in strong asymmetric features in the measurements. No such deviations were observed in any of the experiments, indicating that the mean flow variations did not affect the measurements in any detectable manner.

Measurements of the mean velocity profile at different spanwise and streamwise locations showed that the flow conformed to the Blasius solution, but that slight adjustments had to be made to the virtual origin, x_v, of the flow in order to obtain collapse of the data in the Blasius variables. More details concerning these measurements may be found in Breuer, Haritonidis & Landahl (1989) and Cohen, Breuer & Haritonidis (1990). The measurement of the mean flow was recently repeated in its entirety and it was determined that the existence of the virtual origin, which increased with downstream distance, was the result of a very slight positive pressure gradient. By normalizing the measured mean velocity profiles with solutions of the Falkner–Scan equation, using a free-stream velocity given by $U_\infty(x) = U_0(x/x_0)^{0.0035}$, an excellent collapse of the data was achieved at all streamwise stations. It should be noted that this value of the exponent for the free-stream velocity corresponds to an increase in U_∞ of less than 0.4% over the streamwise range of the experiments, a change so small that the Blasius assumption is most probably still valid. However, the possible effects of this slight positive pressure gradient will be discussed in later sections.

3.3. *Flow parameters*

Most of the experiments were conducted at a free-stream velocity, U_∞, of 6 m/s. As mentioned above, the disturbance generator was located at $x_0 = 0.76$ m. Assuming that the mean flow can be described locally by the Blasius solution for the boundary layer, we can calculate the relevant flow parameters at $x_0 = 0.76$ m. These are given in table 1.

3.4. *Experimental procedure*

The structure of the disturbed flow, created by the membrane movement, was mapped out by positioning the hot-wire probe at several (x, y, z) positions downstream of the membrane and measuring the velocity trace as the disturbance

advected past the probe. The measurement sequence was initiated by a pulse from the computer which triggered the membrane motion. After waiting a preset time, the velocity record, consisting of 512 points, was digitized at a rate sufficient to capture the disturbance signal (typically about 300 μs). By measuring at several locations, a complete map of the structure could be assembled. Two kinds of flow maps were obtained by this procedure. By positioning the probe at $z = 0$ and at several y-locations through the boundary layer, a vertical slice through the disturbance at the centreline of the structure was obtained. Measurements were taken at 20 y-positions through the boundary layer spanning a vertical height of $5\delta^*$. The vertical spacing was arranged according to a 1.5 power law so that there was increased resolution near the wall.

The second mapping that was performed determined the spanwise structure of the disturbance. This was measured with a V-shaped hot-wire probe, measuring both u and w at a fixed height in the boundary layer. The probe was positioned at a height where $u/U_\infty = 0.3$, which corresponds to $y/\delta^* \approx 0.5$. The disturbance was mapped out in the (t, z)-plane by taking measurements at 33 spanwise locations, evenly spaced at $1\delta^*$ intervals and spanning $z = \pm 16\delta^*$. Both of these flow mappings produced similar plots to those shown in the previous numerical results with the exception that t, instead of x, is depicted on the horizontal axis. From these two kinds of mapping, a good representation of the complete structure could be inferred. These measurements were carried out at several different x-locations, starting at $\Delta x/\delta^* = 8.5$ downstream from the membrane location and thereafter at regular intervals of approximately $8.5\delta^*$.

At each (x, y, z) position, 100 realizations of the disturbance's passage were measured and an ensemble average was then calculated. In all cases, the disturbance velocity was extremely coherent, and so the ensemble average is a very faithful representation of an individual realization. The averaging process was beneficial in reducing the random background noise. This was especially important at the edges of the disturbance, where the perturbation velocities were very weak and of the same order as the random background noise and the averaging was necessary to pick out the coherent signal from the incoherent fluctuations present in the flow.

All three components of velocity were initially measured but several problems with the measurement of the v-component were encountered and these results had to be discarded. The problems in measuring v were associated with the contamination of the ×-probe data by the spanwise velocity component of the disturbance and the strong spanwise shear layers in the streamwise velocity, $\partial u/\partial z$. Since u and w are of similar order, while v is an order of magnitude smaller, both the spanwise velocity and the strong spanwise gradients in u contributed to the creation of 'phantom' v-signals which were of the same order as the real v that we were attempting to measure. This contamination was evident, for example, when the measured v was observed to be antisymmetric in z when it should have been symmetric (the u-component is symmetric and the w-component is antisymmetric). The mechanism for the contamination of the v-signal was tested by subjecting the ×-probe to a steady cross-flow and observing the measured u- and v-components. While the u-component remained accurate, the v-component (which should have remained at zero) indicated a small 'phantom' value. Similarly, by rotating the ×-probe and placing it in boundary layer so that it measured the u- and w-components, it was found that a phantom spanwise velocity was detected, induced by the gradient in the streamwise velocity. Similar problems were noticed by Gresko (1988) using an ×-probe in a turbulent boundary layer.

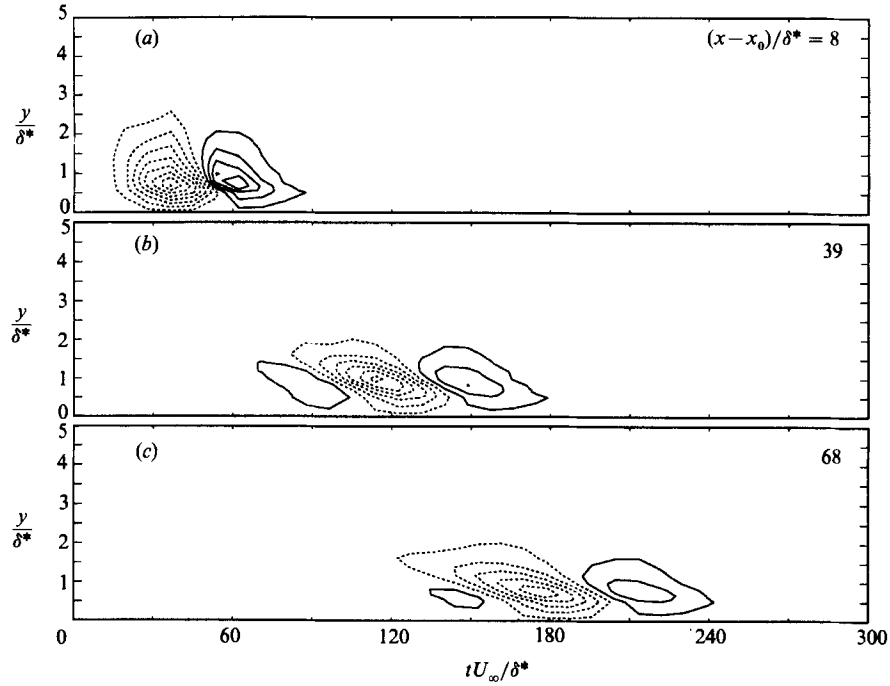

FIGURE 7. Experimental data. Contours of streamwise perturbation velocity in the (t, y)-plane at $z = 0$. Contour spacing: $0.0025U_\infty$.

3.5. *Results and discussion*

3.5.1. *Streamwise disturbance velocities*

Contours of the streamwise velocity perturbations in the (t, y)-plane at $z = 0$ are shown in figure 7 (*a–c*). These are representative of measurements made at several downstream stations. In this figure, as before, the disturbance is plotted with the local mean velocity subtracted. Time is plotted along the horizontal axis and so the structure of the disturbance may be inferred via a frozen-flow assumption. The validity of this assumption depends on the slow development of the disturbance in relation to the speed at which it advects past the hot-wire probe. As figure 7 shows, the disturbance does not change very much from station to station, indicating that this assumption is valid. The structure of the streamwise disturbance is very similar to the structure calculated by the linear theory. The liftup of low-speed fluid by the membrane's upward motion and the subsequent pulldown of high-speed fluid by the membrane's return motion creates two adjoining regions of locally decelerated and accelerated fluid. These two patches of fluid are advected by the local mean velocity which quickly results in the formation of the inclined shear layer: even at the first measuring station ($\Delta x/\delta^* = 8.5$) the tilting of the shear layer is evident. At successive downstream stations, the disturbance tilts with an increasingly acute angle of inclination to the wall, intensifying the shear layer accordingly. By $\Delta x/\delta^* = 42$, the inclination angle and the thickness of the shear layer seem to have reached an equilibrium level at which point the forcing by the mean shear might be offset by viscous forces, which set a limit on the intensity of the shear layer. After decreasing slightly from a maximum of 3 % of U_∞ at the first measuring station, the disturbance amplitude remains relatively constant at about 2 % of U_∞ as the structure moves downstream.

Although the calculations of §2 were linear and inviscid, the qualitative agreement between those results and the measurements is nevertheless quite good. The formation of the inclined shear layer and the confinement of the structure to the region of mean shear both indicate that the mechanism governing the initial evolution of the viscous disturbance is the same as its inviscid counterpart, namely the generation of vertical vorticity by the three-dimensional liftup effect. In the inviscid calculations, the streamwise disturbance amplitude increased with time as a result of the continued liftup of fluid by the vertical perturbation velocity. Only when v decayed did the u-fluctuations level off to a constant amplitude. Since the measured u does not exhibit any continued growth in amplitude, we can assume that the initial vertical displacement velocity due to the membrane motion must decay quite rapidly so that the liftup process ends very soon after the initial generation point and the disturbance reaches a maximum amplitude after a very short time. Despite its constant amplitude, however, the disturbance continues to grow as it advances downstream by virtue of its elongation. During this time its length increases linearly from about $25\delta^*$ at $\Delta x/\delta^* = 17$ to about $40\delta^*$ at $\Delta x/\delta^* = 68$. Thus, although the perturbation velocity remains constant, the energy of the disturbance nevertheless grows as the structure increases in size. This behaviour is also consistent with the inviscid results. Since the transient travels at the local mean velocity, we would expect that the length of the disturbance will grow linearly with time. This 'growth by elongation' is precisely the algebraic instability discussed by Landahl (1980).

However, the association between the viscous and the inviscid results should not be taken too far and there are significant differences between these results and the inviscid calculations. In the viscous flow, the vertical vorticity modes are actually damped (Benney & Gustavsson 1981) and as the generation of vertical vorticity by the liftup process ends, the transient begins to slowly decay as the disturbance travels downstream. The residue of the disturbance is the contribution from the unstable Orr–Sommerfeld modes which form a slowly growing wave packet. This is illustrated in figure 8 which shows the u-component of velocity measured on the centreline at several x-locations, ranging from a station immediately behind the membrane to a station far downstream at $\Delta x/\delta^* = 300$. As before, the pattern behind the membrane reflects the motion of the membrane. The up–down motion creates a low-speed–high-speed velocity perturbation in the streamwise velocity signal. For this case, the initial perturbation amplitude was chosen to be quite small, and the peak-to-peak amplitude of the first u-signal is only 0.8% of U_∞. This decreased amplitude (compared with figure 7) enables us to distinguish more clearly between the advective and wave parts of the disturbance and it lessens the weak nonlinear effects that were observed (it does not completely eliminate them). However, it also means that the disturbance becomes more difficult to measure experimentally because of its very low amplitude. As the disturbance moves downstream, the transient stretches and slowly decays, and at an x-location of about $\Delta x/\delta^* = 200$ the disturbance is comprised solely of a wave packet. By measuring the peak-to-peak amplitude of the disturbance at these x-locations, it was found that the growth of the wave packet is exponential, with a growth rate of about 0.005. This is in reasonable agreement with the theoretically predicted value of about 0.01 (Jordinson 1970) for a zero-pressure-gradient boundary layer. The lower growth rates of the Tollmien–Schlichting waves may be partially accounted for by taking into account the observed slight pressure gradient in the mean flow. If one solves the Orr–Sommerfeld equation, using the appropriate Falkner–Scan profile, one finds

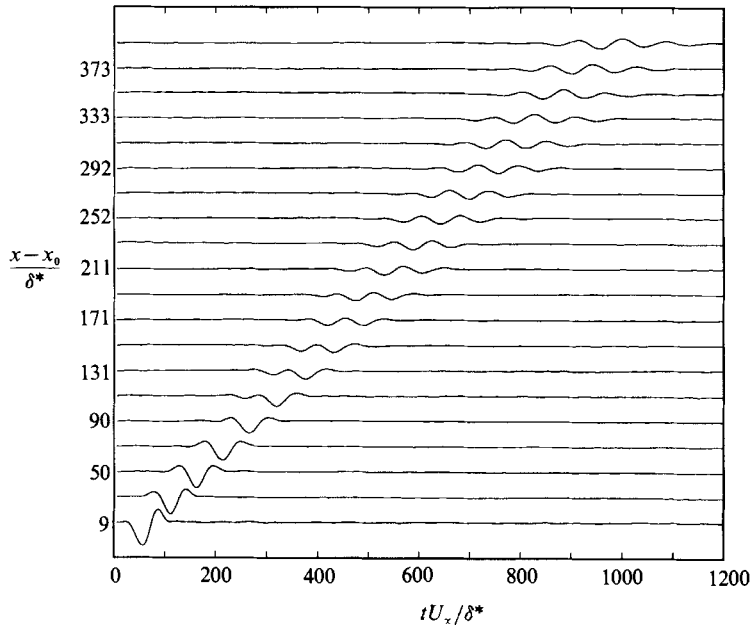

FIGURE 8. Experimental data. Evolution of streamwise velocity at $z = 0$ and $y/\delta^* = 0.5$ showing transition from transient-dominated to wave-packet regimes.

that the maximum spatial growth rate decreases from the Blasius value of 0.010 to a value of 0.009, in somewhat better agreement with the present results.

By following distinctive features we can estimate propagation speeds at the different stages of the evolution of the disturbance. The density of measurements in the downstream direction, as well as the degree to which these features lie on a straight line, yield accurate values for these propagation speeds, and even if the absolute values are susceptible to small errors, the relative differences in speed are still valid. Close to the point of generation, the trough in the disturbance velocity was found to travel at a speed of $0.38U_\infty$. This is somewhat high for the transient part, given that the local fluid velocity at this height in the boundary layer is $0.30U_\infty$. However, in the wave-packet stage, the wave speed was found to be $0.34U_\infty$ while the dominant frequency was found to be 0.08, both in very good agreement with the predicted values of the most-amplified Tollmien–Schlichting wave for the appropriate Falkner–Scan boundary layer at that Reynolds number, which were calculated to be $0.33U_\infty$ and 0.081 respectively. The leading and trailing edges of the wave packet were found to propagate at $0.37U_\infty$ and $0.45U_\infty$ respectively, in excellent agreement with the envelope speeds measured by Gaster & Grant (1975).

The spanwise structure of the disturbance is shown in figure 9. The structure of the disturbed flow field immediately behind the disturbance generator again reflects the motion of the membrane and is typical of the advective description of the localized disturbance. The regions of low-speed fluid, followed by high-speed fluid are consequences of the up–down motion of the membrane pushing up and pulling down fluid particles in the boundary layer. Small lobes are also seen on either side of the central perturbations. These too are natural consequences of the membrane's initial movement. The positive v caused by the membrane's upward motion is accompanied by a weaker negative v on either side, necessitated by continuity. In an identical manner to the central motion, this downward motion brings with it high-speed fluid

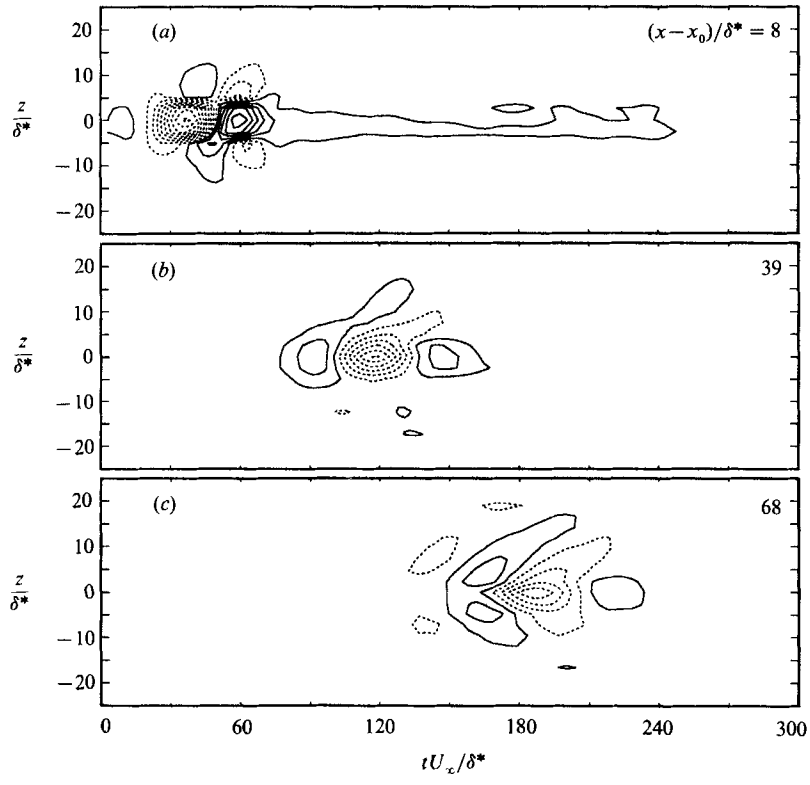

FIGURE 9. Experimental data. Contours of streamwise velocity in the (t,z)-plane at $y/\delta^* = 0.5$. Contour spacing: $0.0005U_\infty$.

from the upper flow, resulting in a small region of locally accelerated fluid. That the initial flow pattern in figure 9(*a*) so closely matches the results from the inviscid calculations of the previous section (figure 5*a*) again indicates that the analytic initial conditions chosen were a good approximation of the disturbance actually produced by the membrane.

As we progress downstream, the evolution of the disturbance is observed in figure 9(*a–c*). By $\Delta x/\delta^* = 39$ the distinction between the advective and the dispersive parts of the disturbance becomes clear. As was seen in the inviscid calculations, the central core of the structure forms the advective part while the wave structure becomes more apparent at the edges of the disturbance and at later x-locations. The dispersive part begins to grow, forming the swept-back wave packet familiar from the results of Gaster (1975) and Gaster & Grant (1975). These waves have a typical frequency which agrees well with the frequency of the most unstable mode at that local Reynolds number. Further downstream, the transient part continues to decay, while the accompanying waves grow and disperse as they propagate downstream. Since the membrane is symmetric about the x-axis, the disturbance should also show reflective symmetry. This symmetry is initially very good, but there are some differences in the amplitude of the structure on either side of the plane of symmetry. These differences are particularly noticeable in figure 9(*b*). However, since the measurements at subsequent x-locations seem to recover their symmetry, it is safe to assume that the actual disturbance does maintain symmetry fairly well, and that the apparent asymmetric features in figure 9(*b*) are due to experimental inaccuracies.

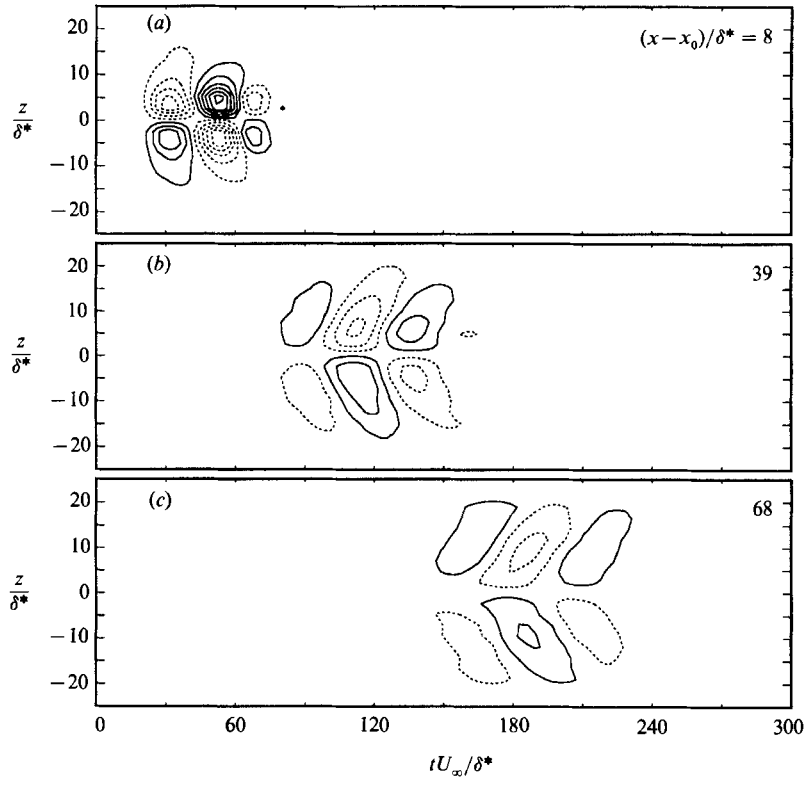

FIGURE 10. Experimental data. Contours of spanwise velocity at $y/\delta^* = 0.5$. Contour spacing: $0.0005U_\infty$.

One comment should be made concerning the long 'tail' behind the disturbance seen in figure 9(*a*). This tail is not a spurious consequence of experimental noise, but rather can be explained as being part of the transient disturbance. Since the advective part travels with the local mean velocity, there is a part of the disturbance, next to the wall, which does not propagate at all but rather remains at the point of generation. Thus, as the disturbance travels downstream, it is in fact 'pinned' to the wall at $x = x_0$, and stretched out from that point. The tail that figure 9(*a*) shows is the evidence of this pinning. After the main disturbance has passed by, the slow-moving and weak tail still remains until it is dissipated by viscosity. At the subsequent downstream x-locations, we should still be able to see the tail, but because of its very low amplitude it has already dissipated and is no longer visible.

3.5.2. *Spanwise disturbance velocities*

The structure of the spanwise velocity component is shown in figure 10. As with the streamwise perturbation, the structure of the w-component at $\Delta x/\delta^* = 8$ strongly reflects the initial generation mechanism and the consequences of the liftup effect. As discussed above, the upward motion of the membrane generates a positive v-velocity and continuity dictates that accompanying this must be a downward motion on either side of the central core. This pattern implies that there must be an accompanying spanwise flow which converges towards the centreline at the bottom of the disturbance structure and diverges from the centreline higher up in the boundary layer. At $y/\delta^* = 0.5$ (where the measurements were taken), which is low in

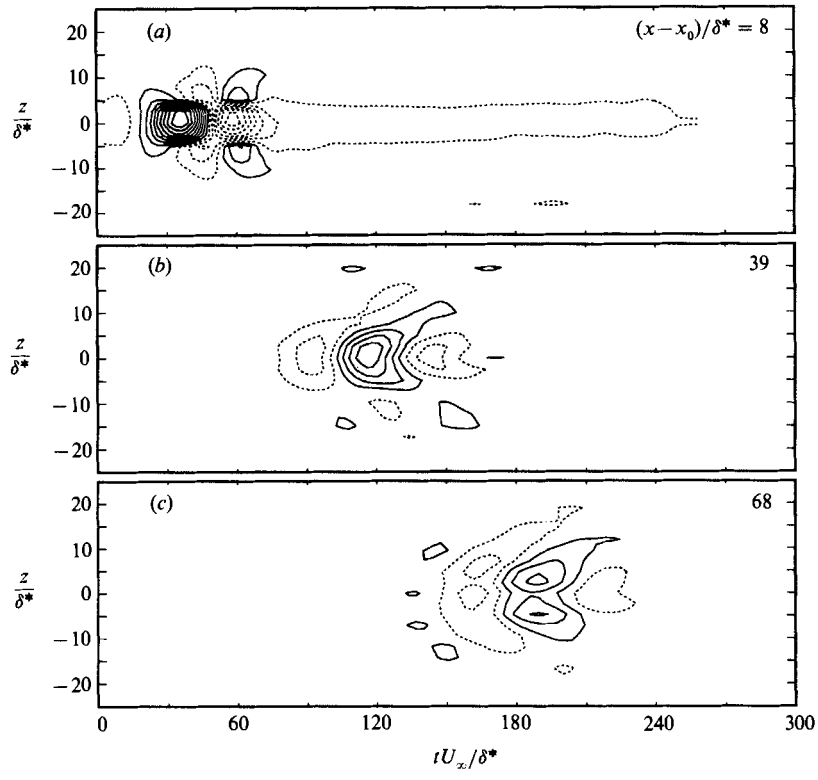

FIGURE 11. Experimental data. Contours of streamwise velocity at $y/\delta^* = 0.5$. *Negative* disturbance (created by a down–up motion of the membrane, instead of an up–down motion). Contour spacing: $0.0005U_\infty$.

the boundary layer, a positive streamwise perturbation should therefore be accompanied by a converging flow and, conversely, the downward membrane motion, resulting in a positive streamwise perturbation should be accompanied by a diverging spanwise flow. Indeed, this is what is observed in figure 10(*a*). As with the streamwise velocity perturbations, the w-component changes as the disturbance progresses downstream from the compact format of the advective modes, to the swept-back and more extensive pattern of the wave packet. The typical frequency of the w-perturbation also changes from one associated with the membrane size to the lower frequency associated with linear instability waves. It is interesting to note that although the linear theory predicts that both horizontal velocities will reflect the liftup effect, only the streamwise component exhibits the dramatic shear-layer structure while the spanwise component has a much more smooth appearance. The antisymmetry of the w-component of velocity is expected for a disturbance which is symmetrical in the u- and v-components with respect to its centreline and the experimental results show this antisymmetry with remarkable accuracy.

3.5.3. *Nonlinear effects*

It has already been mentioned that the disturbance observed in figure 7 exhibited some weak nonlinear effects that resulted in the constant amplitude of the streamwise perturbation velocity. In addition to this, figure 9(*c*) shows some nonlinear effects in the appearance of the two peaks on either side of the centreline,

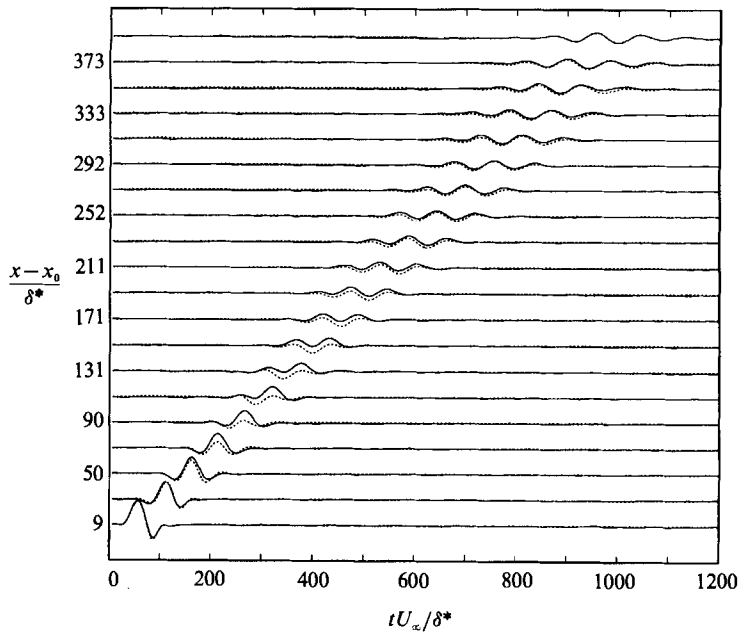

FIGURE 12. Experimental data. Spatial evolution of two disturbances at $z = 0$ and $y/\delta^* = 0.5$. Solid line represents 'positive' disturbance created by an up–down membrane motion while the dotted line represents the 'negative' disturbance, created by a down–up membrane motion. The signal of the negative disturbance is inverted to facilitate comparison.

qualitatively similar to those observed in the late stages of the evolution of the linear wave packet by Gaster & Grant (1975) who also speculated that this was probably due to nonlinear effects. In order to examine these in some more detail the experiments were repeated, creating the same initial disturbance as before, with the same initial amplitude, but with opposite sign. Physically, this was accomplished by operating the membrane with a vacuum source in place of the usual pressure source. The structure of this 'negative' disturbance is seen in figure 11, which shows contours of the streamwise perturbation velocity plotted in the (t, z)-plane. The initial velocity perturbations are almost identical in structure and amplitude but with opposite sign to those in figure 9. The similarity includes the initial structure of the disturbance, the decay of the advective modes, the growth of the wave modes, and the weak tail pinned to the wall behind the disturbance. However, close examination of the later x-locations reveals that, for both signs of initial disturbance, at $\Delta x/\delta^* = 68$ the positive perturbations have split into two peaks off the centreline while the negative perturbations remain centred at $z = 0$. These nonlinear effects are only seen in the streamwise velocity component, and no measurable differences were apparent in the w disturbance velocity.

The weak nonlinearity is again evident in figure 12, in which the centreline streamwise velocity perturbation seen in figure 8 (created by the normal up–down membrane motion) is replotted. Superposed on top of this, plotted with a dotted line, is the centreline streamwise velocity perturbation of the negative disturbance (created by a down–up membrane motion), and *inverted* so as to highlight the similarities and differences between the two disturbances. Initially, in agreement with the contour plots of figures 9 and 11, the two disturbances are identical in structure, but with opposite sign. However, by $\Delta x/\delta^* = 50$, differences between the

two have appeared, and the effect of the nonlinearity is apparent. As the transient decays, and the wave modes establish themselves as the remnant of the initial disturbance, the differences disappear and by $\Delta x/\delta^* = 252$ the wave packets are again identical and opposite. The nature of the nonlinearity is clearly not strong and does not have a global effect on the disturbance since the linearly unstable wavenumbers which remain after the transient has decayed are not affected by the nonlinear action, which was confined to the damped modes of the transient part of the disturbance. It should be noted that the observed nonlinear effects may be connected to variations in the mean flow which might 'trigger' the nonlinearity or provide some mechanism for scale selection. However, since the variations in δ^* are not symmetric about the centreline, and the observed nonlinearities are observed to be symmetric, the effect of the mean flow is thought to be minimal.

4. Conclusions

The importance of three-dimensionality in the evolution of a disturbance has long been acknowledged in the context of secondary instabilities and the later stages of transition. However, in this work we have shown how these mechanisms are not confined to the nonlinear development of the flow, but rather they are *linear* interactions between the vertical velocity in the disturbance, and mean shear of the background flow and as such may be seen at any stage of the transition process. The presence of three-dimensionality in the initial disturbance allows the generation of vertical vorticity which creates the large-amplitude transient, travelling at the local mean velocity, resulting in the inclined shear layer. The agreement between the results of inviscid calculations (in which all modes are either neutrally stable or damped) and measurements in an unstable boundary layer serve to emphasize that this effect is not related to a traditional Tollmien–Schlichting instability mechanism. This effect is quite distinct from the wave packet that also accompanies the disturbance, which is characterized by a substantially lower amplitude and by its vertical coherence and dispersive nature.

The structures that have been seen here, despite their inherent linear nature, strongly resemble the shear layers that have been observed in studies of secondary instabilities (e.g. Klebanoff *et al.* 1962; Kovasznay *et al.* 1962). The resemblance is not by chance, since the present results distill the essential mechanisms that have been found to be important in the secondary instability studies. Herbert (1984) has found that the three-dimensional secondary instability which grows from a finite-amplitude two-dimensional Tollmien–Schlichting wave involves the excitation of the 'Squire modes' – the same vertical vorticity modes that, in this case, are excited by the three-dimensional nature of the initial disturbance. Similarly, the vortex tilting and stretching mechanism described by Stuart (1965) and by Orszag & Patera (1983) can also be thought of in terms of the excitation of vertical vorticity. Both of these mechanisms are present in the localized disturbance, indicating that it is the introduction of three-dimensionality that produces these structures, not directly the amplitude of the perturbed flow.

The present work has been limited to the understanding of the basic linear mechanisms, and thus the disturbances considered in the experiments were of low amplitude. Although the inviscid theory allows for the continued growth of the disturbance, viscosity acts to dissipate the transient so that, far downstream, all that remains is the slowly growing linear wave packet (in fact, by altering the structure of the initial perturbation, one can create disturbances with very different rates of

transient decay). However, it is easy to anticipate what will result if viscosity cannot act quickly enough to dissipate the shear-layer structure. At a higher Reynolds number, or if the initial amplitude is high enough, the shear layer will be sufficiently strong and long lasting that it will not decay, but rather will itself become unstable to shear-layer instabilities and strong nonlinear effects leading to the rapid breakdown of the disturbance. This scenario is discussed in the accompanying paper (Breuer & Landahl 1990).

The advice of Jacob Cohen in the course of this research has been invaluable and is gratefully acknowledged. The authors would like to thank Jorgen Olsson for repeating the entire mean flow measurements, originally done in collaboration with Jacob Cohen. Thanks are also extended to Marten Landahl and Lawrence Gresko for their contributions, and to the referees whose comments have been most helpful. This research was supported by ONR contract N00014-87-K-0048, AFOSR contract F49620-83-C-0019, and the ONR Graduate Fellowship Program. One of the authors (K.S.B.) would like to acknowledge the support of the Center for Fluid Mechanics at Brown University, supported by DARPA-URI grant N00014-86-K-0754.

REFERENCES

AMINI, J. & LESPINARD, G. 1982 Experimental study of an 'incipient spot' in a transitional boundary layer. *Phys. Fluids* **25**, 1743–1750.

ANTAR, B. N. & BENEK, J. A. 1978 Temporal eigenvalue spectrum of the Orr–Sommerfeld equations for the Blasius boundary layer. *Phys. Fluids* **21**, 183–189.

BENNEY, D. J. & GUSTAVSSON, L. H. 1981 A new mechanism for linear and nonlinear hydrodynamic instability. *Stud. Appl. Maths* **64**, 185–209.

BREUER, K. S., HARITONIDIS, J. H. & LANDAHL, M. T. 1989 The control of localized disturbances in a boundary layer through active wall motion. *Phys. Fluids* **3**, 574–582.

BREUER, K. S. & LANDAHL, M. T. 1990 The evolution of a localized disturbance in a laminar boundary layer. Part 2. Strong disturbances. *J. Fluid Mech.* **220**, 595–621.

CASE, K. M. 1960 Stability of inviscid plane Couette flow. *Phys. Fluids* **3**, 143–148.

COHEN, J., BREUER, K. S. & HARITONIDIS, J. H. 1990 On the evolution of a wave packet in a laminar boundary layer. *J. Fluid Mech.* (submitted).

CRAIK, A. D. D. 1971 Nonlinear resonant instability in boundary layers. *J. Fluid Mech.* **50**, 393–413.

DIPRIMA, R. C. & HABETLER, G. J. 1969 A completeness theorem for non-selfadjoint eigenvalue problems in hydrodynamic stability. *Arch. Rat. Mech. Anal.* **32**, 218.

DRAZIN, P. G. & REID, W. H. 1981 *Hydrodynamic Stability*. Cambridge University Press.

GASTER, M. 1975 A theoretical model for the development of a wave packet in a laminar boundary layer. *Proc. R. Soc. Lond.* A **347**, 271–289.

GASTER, M. & GRANT, I. 1975 An experimental investigation of the formation and development of a wave packet in a laminar boundary layer. *Proc. R. Soc. Lond.* A **347**, 253–269.

GRESKO, L. S. 1988 Characteristics of wall pressure and near-wall velocity in a flat plate turbulent boundary layer. *FDRL Rep.* 88-2. Department of Aeronautics and Astronautics, Massachusetts Institute of Technology.

GROSCH, C. E. & SALWEN, H. 1978 The continuous spectrum of the Orr–Sommerfeld equation. Part 1. The spectrum and the eigenfunctions. *J. Fluid Mech.* **87**, 33–54.

GUSTAVSSON, L. H. 1978 On the evolution of disturbances in boundary layer flows. *Trita-Mek*-78-02. Department of Mechanics, Royal Institute of Technology, Stockholm.

HENNINGSON, D. S. 1988 The inviscid initial value problem for a piecewise linear mean flow. *Stud. Appl. Maths* **78**, 31–56.

HERBERT, T. 1984 Analysis of the subharmonic route to transition in boundary layers. *AIAA* 84-0009.

JORDINSON, R. 1970 The flat plate boundary layer. Part 1. Numerical integration of the Orr–Sommerfeld equation. *J. Fluid Mech.* **43**, 801–811.

KLEBANOFF, P. S., TIDSTROM, K. D. & SARGENT, L. M. 1962 The three-dimensional nature of boundary layer instability. *J. Fluid Mech.* **12**, 1–34.

KOVASZNAY, L. S. G., KOMODA, H. & VASUDEVA, B. R. 1962 Detailed flow field in transition. In *Proc. 1962 Heat Transfer and Fluid Mechanics Institute, Stanford University*, pp. 1–26.

LANDAHL, M. T. 1975 Wave breakdown and turbulence. *SIAM J. Appl. Maths* **28**, 735–756.

LANDAHL, M. T. 1980 A note on an algebraic instability of inviscid parallel shear flows. *J. Fluid Mech.* **98**, 243–251.

LANDAHL, M. T. 1984 Coherent structures in turbulence and Prandtl's mixing length theory. *Z. Flugwiss. Weltraumforsch.* **8**, 233–242.

LIN, C. C. 1955 *Theory of Hydrodynamic Stability*. Cambridge University Press.

LUEPTOW, R., BREUER, K. S. & HARITONIDIS, J. H. 1988 Computer-aided x-wire calibration using a look-up table. *Expts Fluids* **6**, 115–118.

MACK, L. M. 1976 A numerical study of the temporal eigenvalue spectrum of the Blasius boundary layer. *J. Fluid Mech.* **73**, 497–520.

MANGUS, J. F. 1984 Preliminary measurements of drag and bursting frequency in a manipulated turbulent boundary layer. *FDRL Rep.* 84-2. Department of Aeronautics and Astronautics, Massachusetts Institute of Technology.

ORR, W. M. F. 1907 The stability of the steady motions of a perfect liquid and of a viscous liquid. Part I: A perfect liquid. Part II: A viscous liquid. *Proc. R. Irish Acad.* A **27**, 9–138.

ORSZAG, S. A. & PATERA, A. T. 1983 Secondary instability of wall-bounded shear flows. *J. Fluid Mech.* **128**, 347–385.

RUSSELL, J. M. & LANDAHL, M. T. 1984 The evolution of a flat eddy near a wall in an inviscid shear flow. *Phys. Fluids* **27**, 557–570.

STUART, J. T. 1965 The production of intense shear layers by vortex stretching and convection. *AGARD Rep.* 514.